Palaeogeography, Palaeoclimatology, Palaeoecology 304 (2011) 74–84

Contents lists available at ScienceDirect

Palaeogeography, Palaeoclimatology, Palaeoecology

journal homepage: www.elsevier.com/locate/palaeo

Defining the timing and duration of the Kačák Interval within the Eifelian/Givetian boundary GSSP, Mech Irdane, Morocco, using geochemical and magnetic susceptibility patterns

Brooks B. Ellwood [a,*], Thomas J. Algeo [b], Ahmed El Hassani [c], Jonathan H. Tomkin [d], Harry D. Rowe [e]

[a] Louisiana State University, Department of Geology and Geophysics, E235 Howe-Russell Geoscience Complex, Baton Rouge, LA 70803, United States
[b] Department of Geology, University of Cincinnati, Cincinnati, OH 45221-0013, United States
[c] Institut Scientifique, Université Mohammed V Agdal, B.P.703 Rabat-Agdal, 10106 Rabat, Morocco
[d] School of Earth, Society, and Environment, University of Illinois, 428 Natural History Building, 1301 W. Green Street, Urbana, IL 61801, United States
[e] Department of Earth and Environmental Sciences, University of Texas at Arlington, Arlington, TX 76019, United States

ARTICLE INFO

Available online 16 October 2010

Keywords:
Eifelian–Givetian boundary
Magnetic susceptibility (MS)
Climate cyclicity
Time-series analysis
Kačák bio-event
Pumilio bio-event

ABSTRACT

Here we present new geochemical and magnetic susceptibility (MS) data from the Global boundary Stratotype Section and Point (GSSP) for the Middle Devonian Eifelian–Givetian (E–G) boundary at Mech Irdane in the Anti-Atlas Mountains of eastern Morocco. These data come from 395 samples collected over a stratigraphic interval of ~20 m, beginning ~4.5 m below the boundary and extending to the Upper *pumilio* marker bed ~14.5 m above the boundary. MS data show long-term transgressive–regressive (T/R) eustatic cyclicity upon which is superimposed shorter-term climate cyclicity. Fourier analysis of these data yield high power at four frequencies that are consistent with Milankovitch–band orbital forcing: eccentricity (E1 and E2) at ~400 and ~100 kyr, obliquity (O1) at ~32 kyr, and precession (P2) at ~20 kyr, the latter two corrected for secular changes in Earth's orbit since the Middle Devonian. A floating-point time scale (FPTS) for the boundary interval has been developed using a P2 cyclicity that allows temporal resolution to ~10 kyr within the section. Based on the stratigraphic ranges of geochemical and MS anomalies, as well as previously reported biostratigraphic extinctions from the boundary interval, we estimate the Kačák Interval to extend from ~1.0 m below the E–G boundary to ~1.0 m above it, with a duration of.~200 ± 10 kyr. Geochemical proxies demonstrate that the Kačák Interval was characterized by more reducing conditions, greater organic carbon burial, and an increase in the flux of detrital materials (especially clays), reflecting an increase in subaerial weathering rates. The *pumilio* beds, located ~12–15 m above the E–G boundary, were deposited during successive maximum highstands under conditions of elevated primary productivity and reduced detrital influx.

1. Introduction

The Eifelian–Givetian (E–G) boundary of the Middle Devonian is well studied (e.g., House, 1985; Walliser, 1991, 1996, 1999; Walliser et al., 1995). The Global boundary Stratotype Section and Point (GSSP) for the boundary, located in Morocco (Fig. 1), was formally ratified by the International Commission on Stratigraphy (ICS) of the International Union of Geological Sciences (IUGS) in 1994. The specifics of the E–G GSSP were published in *Episodes* by Walliser et al. (1995). Based on biostratigraphic studies, this and other work has identified a global environmental/biological disturbance that began just below the boundary and extends to some level above the boundary (House, 1985; Walliser, 1996, 1999; Walliser et al., 1995). This disturbance has been variously named the *otomari* or L'Ei 1 Event (Walliser, 1996, 1999) and Kačák Event (House, 1985), and is defined by biostratigraphic or bio- and lithostratigraphic data, respectively. A number of extinctions of conodont species occurred in conjunction with this event, the stratigraphic representation of which is hereafter referred to as the “Kačák Interval”. A second extinction level (L'Ei 2; Walliser, 1996, 1999) above L'Ei 1, has been identified within this interval at which several ammonoid genera became extinct and several conodont and ammonoid taxa also appeared (Barnes et al., 1996; House, 1985; Walliser, 1996, 1999; Walliser et al., 1995).

Based on study of the E–G GSSP section in Morocco, Ellwood et al. (2003) suggested that the extinctions and lithologic changes observed within the Kačák Interval may have been the result of a bolide impact. This conclusion was based mainly on the presence of shocked quartz grains concentrated within Bed 117 at Mech Irdane and in the equivalent bed sampled at two other Moroccan localities, Bou Tchrafine and Rich Haroun. Bed 117 is the only significant shale/

* Corresponding author. Tel.: +1 225 578 3416; fax: + 1 225 578 2302.
E-mail address: ellwood@lsu.edu (B.B. Ellwood).

0031-0182/$ – see front matter © 2010 Elsevier B.V. All rights reserved.
doi:10.1016/j.palaeo.2010.10.012

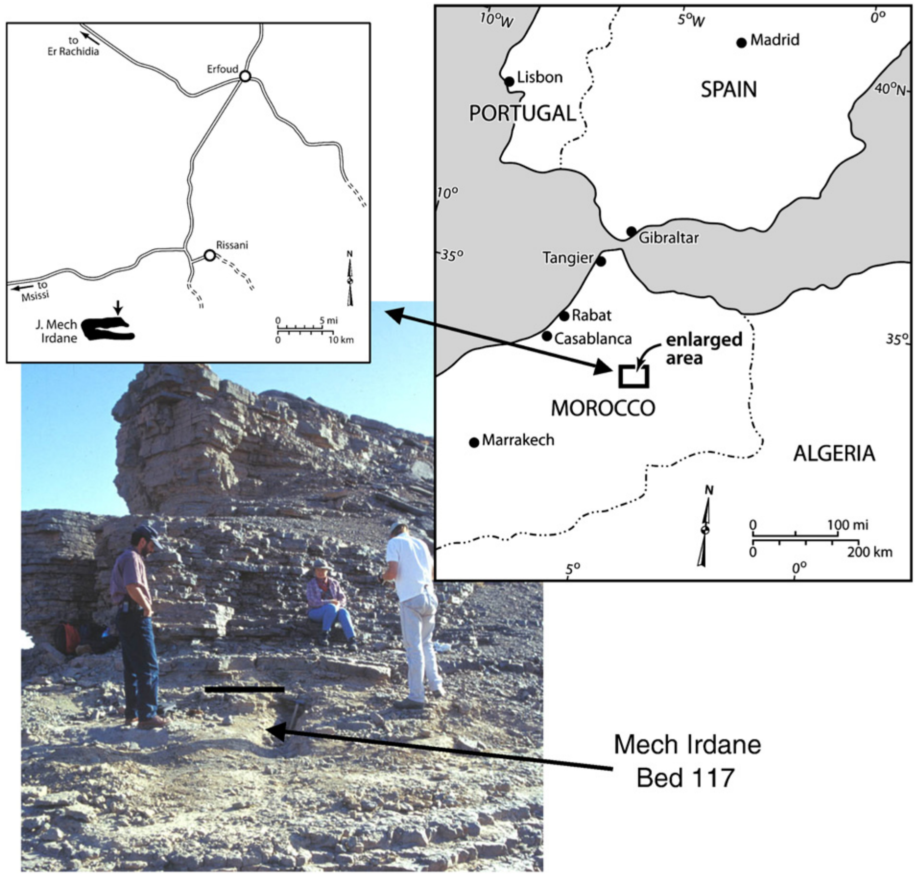

Fig. 1. Location of the Mech Irdane Eifelian–Givetian GSSP near the town of Rissani in the Anti-Atlas desert of Morocco. The section begins ~4.5 m below the E–G GSSP and extends upsection to the distinctive Lower and Upper *pumilio* beds (each ~20 cm-thick and containing high concentrations of small "*Terebratula*" *pumilio* brachiopods and located just below the highest point shown in the figure). The E–G GSSP is located at the black bar below the sitting person; Bed 117 (labeled) lies within the excavated trench between the standing persons.

marl bed in the section (bed numbers from Walliser et al., 1995). However, more recently it has been argued, based on low platinum group element values in marl Bed 117 at Mech Irdane, that this sequence may not represent a bolide impact (Schmitz et al., 2006). In addition to identifying shocked quartz in Bed 117, Ellwood et al. (2003) also reported large geochemical and magnetic susceptibility (MS) variations within the Kačák Interval. These variations represent perturbations within the E–G environment and depict arguably the causal mechanism behind the contemporaneous extinctions.

The purpose of the present study is to better characterize the Kačák Interval in the E–G GSSP at Mech Irdane, including the timing of its onset and termination, its duration, and the mechanism responsible for the large-scale environmental disturbances at the Eifelian–Givetian boundary. Addressing these issues required more extensive sampling of the study section than previously undertaken (for the purpose of time-series analysis), as well as application of additional geochemical proxies in order to more fully characterize environmental changes in the Eifelian–Givetian boundary interval (for the purpose of inferring mechanism). Therefore we returned to Mech Irdane and extended the sample data sets above and below the E–G GSSP to include ~20 m of section. The results of this work are detailed below.

2. Previous work

In order to answer the question of how long the Kačák Interval lasted, we must have a way to initially identify the top and bottom levels of the interval, and to estimate how long it took to deposit these sediments. Geochemical and MS extremes allow for the identification of the interval top and base, but to understand the timing of the interval it is necessary to have a mechanism tied to a methodology that facilitates development of a time scale of sufficient resolution to yield age estimates on the order of less than 500 kyr. This resolution is possible with data sets that produce records or proxies of climate cyclicities. One such proxy comes from isotopic studies (e.g., Imbrie et al., 1984) and another comes from MS cyclicity recorded in sediments (e.g., Weedon et al., 1997).

Isotopic studies of Cenozoic marine sediments/rocks rely on the assumption that isotopic (and cyclic lithologic) changes are a proxy for climatic cycles that are assumed to be global (e.g., Dinarès-Turell et al., 2007; Imbrie et al., 1984). Tests of these hypotheses have shown that, in general, these basic assumptions are correct, and that these data can provide a much higher resolution for time scales than are achievable based only on biostratigraphic information. Such data sets have not been generated for most of the Phanerozoic, however, because stratigraphic sequences are imperfect recorders of time owing to erosion, non-deposition or alteration. As a consequence of these processes, short-term Milankovitch cycles (i.e., Earth's obliquity and precession) are not as well developed in older rocks as they are in younger sequences. It is therefore expected that longer-term climate cycles are more readily identified in older rock sequences, and that at least the ~405 kyr eccentricity cycle has a robust, long-term paleoclimatic signal that should be manifested in stratigraphic successions (Laskar et al., 2004; Shackleton et al., 1999a). This cycle has been observed within Middle Devonian (Ellwood et al., 2011–this volume) and Middle Carboniferous marine sediments (Ellwood et al., 2007b), Triassic lacustrine sediments (Olsen and Kent, 1995), and

Jurassic (Boulila et al., 2008) and late Cretaceous marine sediments (Gale et al., 2008). Given that longer-term climate cycles are preserved in the sedimentary record, any robust method that can track these changes should provide useful proxies for climate and time-series analysis.

One such method that is now well established uses low-field MS data sets in both unlithified and lithified marine sediments to track climate cyclicity. Therefore, the cyclostratigraphic record in these sequences can be used for astronomical calibration of geologic time scales (Crick et al., 2001; Hartl et al., 1995; Mead et al., 1986; Shackleton et al., 1999b; Weedon et al., 1997, 1999). In addition to its utility in paleoclimate studies, MS can be used for high-resolution correlation among marine sedimentary rocks of broadly differing facies with regional and global extent (Crick et al., 2000; Ellwood et al. 2007a,b; Whalen and Day, 2008). MS works as a climate proxy and can be used for correlation because regional and global processes that drive erosion, including climate and eustasy, bring the detrital components responsible for the MS signature into the marine environment where its stratigraphy is preserved (Ellwood et al., 2000).

3. Methods

3.1. Magnetic susceptibility: general comments

All materials are “susceptible” to becoming magnetized in the presence of an external magnetic field, and initial low-field bulk magnetic susceptibility or MS is an indicator of the strength of this transient magnetism. MS in marine stratigraphic sequences is generally considered to be an indicator of detrital iron-containing paramagnetic and ferrimagnetic grains, mainly ferromagnesian and clay minerals (da Silva and Boulvain, 2002; Ellwood et al., 2000, 2008b), and can be quickly and easily measured on small samples. In the very low inducing magnetic fields that are generally applied, MS is largely a function of the concentration and composition of the magnetizable material in a sample. MS can be measured on small, irregular lithic fragments and on highly friable, unoriented sample material that is difficult to sample for other types of measurement.

MS in lithified marine sedimentary sequences mainly records processes that control the influx of detrital grains into the marine environment. Most MS studies of marine sedimentary rocks show many levels of cyclicity with certain cycles interpreted to result from climatically driven processes (Ellwood et al., 2000; Weedon et al., 1999). Other cycles are very longer-term and are interpreted as resulting from transgressive–regressive (T/R) trends due to sea level rise and fall associated with eustacy. As a general rule, especially in distal marine sequences, MS is observed to decrease during transgressive cycles due to detrital sediments being trapped in the near-shore during transgressions. However, there are distinct MS peaks that are correlated to maximum flooding surfaces, as well as to sudden influxes of detrital material into sedimentary basins by turbidity currents or other sediment suspensions. During regressions, when base level is lowered due to falling sea level, erosion flushes detrital sediment into ocean basins and increases the MS of basinal sediments. Thus T/R cycles play an important role in creating some cyclic MS variations observed. It has also been demonstrated that sediment starvation, for example due to the removal of detrital components by winnowing, may significantly reduce MS values (Ellwood et al., 2007a).

3.2. Field sampling

In the field we first cleaned the section using scrapers and brushes, so that all beds and lithologies were well exposed (Fig. 1). Highly weathered zones were cleaned by digging, chipping and brushing. A suite of 395 samples was collected for MS and geochemical measurement at ~5 cm intervals over a distance of ~20 m and returned to the laboratory for study. Geochemical analyses were performed on a subset of 68 samples through an interval extending from 4.5 m below to 6 m above the boundary.

3.3. Magnetic susceptibility analysis

MS measurements reported in this paper were performed using the balanced coil susceptibility bridge at LSU (manufactured by Marshal Williams, University of Georgia Electronics Shop, 1988), and calibrated relative to mass using standard salts reported by Swartzendruber (1992) and CRC Tables. We report MS in terms of sample mass because mass is much easier and faster to measure with high precision than is volume, and it is now the standard for MS measurement.

MS data for most marine sedimentary rocks (>99.9%) range from 1×10^{-9} to 1×10^{-7} m^3/kg. For the purpose of graphic representation, the MS data are presented here as δMS data, where

$$\delta MS = (MS_{measured} - MS_{marine\ standard}) / MS_{marine\ standard} \qquad (1)$$

and $MS_{marine\ standard} = 5.5\times10^{-8}$ m^3/kg, which is the median value for ~11,000 analyses of lithified marine sedimentary rocks, including siltstone, limestone, marl and shale samples measured at LSU. While additional analyses would certainly change slightly the measured median value, it is useful to have a fixed value that reflects a reasonable median for marine sedimentary rocks to which other studies can be compared. Therefore, it is recommended that the value for the MS marine standard of 5.5×10^{-8} m^3/kg be used as a fixed standard for future comparisons when δMS calculations are used.

δMS is useful because it is dimensionless and allows direct comparison to other MS data sets. Given that MS values in marine sedimentary rocks mainly range from ~1×10^{-9} to ~1×10^{-7} m^3/kg, distortions in δMS due to very high anomalous values ($\gg 1\times10^{-7}$ m^3/kg) are visually enhanced, and therefore rapidly identified in these data sets. Extremely low values ($<1\times10^{-9}$ m^3/kg) are generally not well resolved with many instruments, and these low-end extremes are reduced by using δMS. A δMS value of zero is coincident with the $MS_{marine\ standard}$ and therefore equal to the median value of the ~11,000 marine rock samples measured. Negative δMS values are lower than the standard median marine value and positive values are higher. This approach is similar to that used by isotope geochemists, i.e. in calculating $\delta^{18}O$ values, and has a number of advantages when evaluating MS data sets. First, MS magnitude can be directly compared among data sets and between instruments. Second, δMS is a truly dimensionless number, as opposed to direct MS values that require adjustment due to measurement relative to a given sample mass or volume. Third, presentation of MS data with values ranging over more than one order of magnitude is not significantly distorted when plotted, as are normal MS values when presented in either a linear or log plot.

For presentation purposes the bar-log format, similar to that previously established for magnetostratigraphic polarity data presentations, is used here. Bar-logs were constructed from the raw δMS data set. Because δMS data are cyclic, we use a bar-log plotting convention, such that if a δMS cyclic trend is represented by two or more data points, then this trend is assumed to be significant and the highs and lows associated with these cycles are differentiated by black (high δMS values) or white (low δMS values) bar-logs. This method is best employed when high-resolution data sets are being analyzed (large numbers of closely spaced samples). High-resolution data sets help resolve MS variations associated with anomalous samples. Such variations may be due to weathering effects, secondary alteration and metamorphism, to longer-term trends due to factors such as eustasy (Ellwood et al., 2008a), as opposed to shorter-term climate cycles (Ellwood et al., 2007b) or event sequences such as impacts (Ellwood et al., 2003), and other factors. In cases where non-deposition, pressure solution, condensation of section and slight erosion affect the sequence, MS zones are compressed, but the MS character is visually preserved in the MS bar-log, and thus, such effects are readily identified by this compression.

3.4. Time-series analysis using the Fourier Transform (FT) method

In an effort to characterize cyclicity in our data set (395 samples), we have performed a time-series analysis of the MS data for samples from the E–G GSSP. First, we assumed that the spacing of samples is linearly related with time, i.e., Δx (change in spacing) is proportional to Δt (change in time), so that a Fourier method could be used. It is important to note, that the less this assumption is true, the more noise will be produced in the spectral graph, with the result that spectral power is diminished. The spectral power of the MS data sets was obtained with FT analysis. The data were both detrended and subjected to a Hanning window so as to reduce spectral leakage and increase the dynamic range (Jenkins and Watts, 1968). Incidences of statistically significant peaks (at the 95% level) in the resulting spectrum are determined by employing the multi-taper method (Ghil et al., 2002), as calculated with the SSA-MTM toolkit (Dettinger et al., 1995). A null hypothesis of red noise is assumed, with a three taper model in which the harmonic signals were tested against an F-test. This method is prone to producing false positives: the large amount of data examined in this study may produce a spurious 5% signal several times. We therefore restrict the use of statistical significance here to its role in supporting (or not) the positions of multiple Milankovitch bands within the data set.

3.5. Geochemical analyses

Carbon and sulfur elemental concentrations were measured using an Eltra 2000 C-S analyzer at the University of Cincinnati. Data quality was monitored via multiple analyses of the U.S.G.S. SDO-1 standard (TC = 9.68 wt.%; TS = 5.35 wt.%), yielding an analytical precision (2σ) of $\pm 2.5\%$ of reported values for carbon and $\pm 5\%$ for sulfur. An aliquot of each sample was digested in 2 N HCl at 50 °C for 12 h to dissolve carbonate minerals, and the residue was analyzed for total organic carbon (TOC) and non-acid-volatile sulfur (NAVS); total inorganic carbon (TIC) and acid-volatile sulfur (AVS) were obtained by difference.

About 3–4 g of each sample analyzed were pressed into a powder mount and analyzed for whole-rock major- and trace-element concentrations using a wavelength-dispersive Rigaku 3040 XRF spectrometer at the University of Cincinnati. Results were calibrated using both USGS (SDO-1, SCO-1, SGR-1) and internal black shale standards (analyzed using XRF and INAA by XRAL Incorporated). Analytical precision based on replicate analyses was better than $\pm 1\%$ for Zr, Y, and Rb, $\pm 3.2\%$ for Mn, $\pm 3.8\%$ for Na, $\pm 5\%$ for other trace elements, and $\pm 2\%$ for other major and minor elements. Detection limits for trace elements were 5 ppm for Nb, Zr, Y, Sr, Rb, Zn, Cu, and Ni, 15 ppm for Cr and V, 20 ppm for U, and 50 ppm for Ba. Mineralogic compositions of samples were estimated per the procedure of Algeo et al. (2007) using values for κ_1 and κ_2 of 1.2 and 15.0, which were found to minimize variance ($\sigma = 5.9\%$) about a mean sum of 100% for the sample set as a whole.

Stable isotopic compositions ($\delta^{13}C$, $\delta^{18}O$) were analyzed at the University of Kentucky Environmental Research Training Laboratory using a GasBench-II peripheral coupled to a Delta*Plus*XP isotope ratio mass spectrometer. Samples (450 ± 50 µg) were equilibrated at 40 °C for 24 h before analysis. Average precision for $\delta^{13}C$ and $\delta^{18}O$ of NBS-19 calcite standard was 0.05‰ and 0.05‰, respectively, for the entire dataset. Average precision for $\delta^{13}C$ and $\delta^{18}O$ of unknowns was 0.02‰ and 0.05‰, respectively. All results are reported relative to V-PDB.

4. Results

4.1. Magnetic susceptibility

Magnetic susceptibility (MS) was measured for 395 samples collected from the cleaned, E–G GSSP section at Mech Irdane, Morocco (Fig. 1) and δMS is reported in Fig. 2. The GSSP 'point' is located at the base of the feet of the person sitting in Fig. 1, and excavations and cleaning of marl Bed 117 can be seen between the two standing persons. The section extends below that level ~4.0 m and upwards to the crest of the section where two *pumilio* layers (each marked by abundant small brachiopod layers (Lottmann, 1990a,b) have been identified (Fig. 2). From the base of the section to about 6 m above the E–G GSSP, δMS values are slightly higher than the median for most marine rocks, being generally within the range of 0.0 to 0.5, with two exceptions: (1) lower δMS values (<0) just below the base of marl Bed 117, and (2) much higher values (δMS from 0.5 to 2.0) in the ~1.0 m interval just above the boundary (Fig. 2). Above 6 m, δMS values fall below the median for marine sedimentary rocks, with values ranging from 0.0 to −0.8.

4.2. Time-series analysis

The MS profile for the study section (Fig. 2) exhibits distinct cyclicity, as demonstrated by the Fourier Transform (FT) shown in Fig. 3. Through an iterative procedure, we have assigned cycles in the power spectrum to known Milankovitch peaks (Fig. 3). Our best-fit resulted when we assumed that the peak at ~6.2 cycles is the P2 precessional cycle (~20 kyr; shorter than the modern value of ~23 kyr; Berger et al., 1992). This ~20 kyr P2 peak has been used to calculate the length of time, ~2.5 myr, represented by deposition of the entire ~20 m E–G section shown in Fig. 2 (each cycle lasting ~20 kyr in a ~20 m long section with ~6.2 cycles/m). Then, assuming the result for the length of time it took for the Mech Irdane section to be deposited was ~2.5 myr, we can calculate where other Milankovitch peaks should lie. Given that this power spectrum exhibits well-defined peaks at ~0.2–0.3 and 1.2 cycles/m, these then can be linked to the orbital eccentricity cycles E1 (~405 kyr) and E2 (~100 kyr). A smaller, higher frequency peak is present at ~4.0 cycles/m, which is likely to represent the O1 obliquity cycle (~32 kyr; also shorter than the modern value of ~41 kyr owing to secular evolution of the Earth's orbital parameters; Berger et al., 1992). At frequencies higher than ~5 cycles/m, a series of peaks are present, including the one at ~6.2 cycles/m chosen to represent the P2 precessional cycle. The fact that substantial power is present at frequencies between ~5 and 9 cycles/m is consistent with strong precessional forcing of MS variation in the study section, with smearing of the precessional signal as a consequence of both short- and long-term variation in sediment accumulation rates within the study section (Section 4.3). This precessional signal forms the basis for the time model developed in the next section.

4.3. Graphic comparison and the floating-point time scale (FPTS)

Power in the frequency range of ~5 and 9 cycles/m (Fig. 3) is strongly expressed in the MS profile of the study section (Fig. 2). We interpret this signal as a record of climatically driven changes in the fluxes of various detrital components at precessional orbital frequencies (cf. Ellwood et al., 2008a; Weedon et al., 1997). We use the MS bar-log compiled from the raw MS variations from the expanded study section in Fig. 4, through the Kačák Interval, and graphically compare it to a uniform P2 frequency model (the model is built by assigning a constant sediment accumulation rate [SAR] of ~20 kyr/cycle to the x [Floating-Point Time Scale] axis in Fig. 5). In Fig. 5, we have projected the bottoms and tops of corresponding MS bar-log zones for the Mech Irdane MS profile (left) and the P2 frequency model (x axis) and then drawn best-fit "lines of correlation" (LOC)

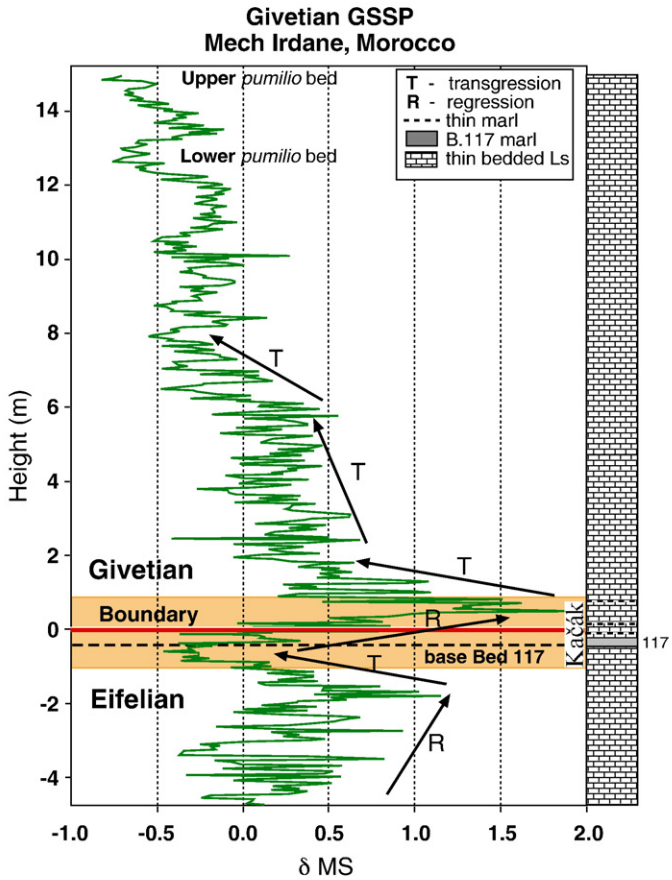

Fig. 2. δMS profile for ~20 m-thick study section based on 395 samples collected at ~5 cm intervals (see Section 3.3 for a definition of δMS). The shaded area represents the stratigraphic extent of the Kačák Interval, an anomalous zone showing unusual geochemical and MS features (see Section 5.1 for a discussion). The E–G boundary level is the red horizontal bar in the figure. The base of Bed 117 is labeled; it is the only significant (~20 cm) marl bed found within the section. The lithologic log indicates the almost complete dominance of thin-bedded limestone in the section.

through those data points that define straight-line segments (similar to the method used by the graphic correlation technique of Shaw, 1964). This procedure resulted in delineation of three trends (A–C in Fig. 5) representing intervals of relatively uniform SAR. Trend A, comprising ~75 cm below Bed 117, yields a SAR of 0.63 cm/kyr. Trend B, comprising ~50 cm from the base of Bed 117 to just below the E–G boundary, yields a SAR of 1.4 cm/kyr. Trend C, comprising ~2.75 m from just below the E–G boundary into the lowermost Givetian, yields a SAR of 0.94 cm/kyr. The increase in SAR represented by trend B is linked to a shift in lithology from limestone to marl (Bed 117), but the onset of a higher SAR commences in the limestones of Beds 114–116, indicating that changes in SAR preceded the probably related changes in lithology. This interval (base of Bed 117) also contains most of the shocked quartz grains identified at Mech Irdane as well as the largest geochemical anomalies observed in the study section (Ellwood et al., 2003; Figs. 6 and 7 of this paper).

The pronounced cyclicity in the MS profile at Mech Irdane allows us to establish a floating-point time scale (FPTS) model based on the assumed uniform P2 orbital frequency model of ~20 kyr (Fig. 3) discussed earlier. This FPTS shows that the ~4 m interval subjected to graphic comparison (Figs. 4, 5) represents a time period of ~450 kyr, and that the Kačák Interval (as redefined in this study) commenced ~90 kyr before the E–G boundary and terminated ~110 kyr after the boundary, with a total duration of ~200 kyr. Furthermore, the petrographic (i.e., marl containing shocked quartz) and large geochemical variations associated with Bed 117 represent an interval of ~10–15 kyr that terminated ~20 kyr prior to the E–G boundary (Fig. 4). This FPTS can also be used to calculate durations for biostratigraphic zones and bioevents identified throughout the study section. This has been done for conodonts for the entire Givetian Stage and covers this interval (see Ellwood et al., 2011–this

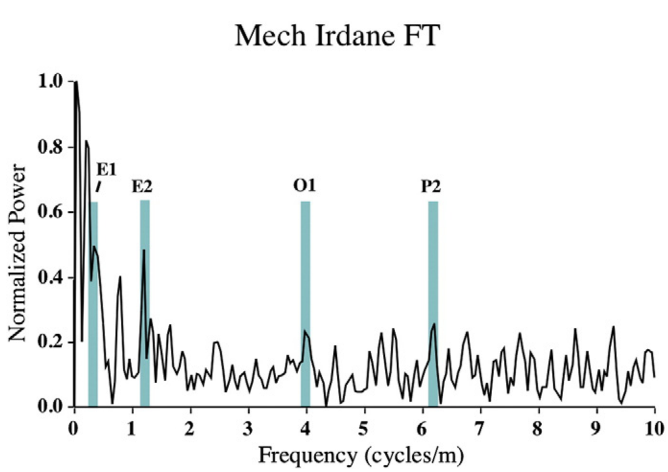

Fig. 3. Time-series analysis, using the Fourier transform (FT) method, of the raw MS data from measurements of 395 samples from the Mech Irdane, Eifelian–Givetian GSSP near Rissani, Morocco (Figs. 1, 2). We identify four Milankovitch cycles, two eccentricity peaks (E1 ~405 kyr; E2 ~100 kyr), one obliquity (O1 ~32 kyr) and one precessional (P2 ~20 kyr). The obliquity and precessional values are corrected for secular changes in Earth's tilt and wobble after the work of Berger et al. (1992).

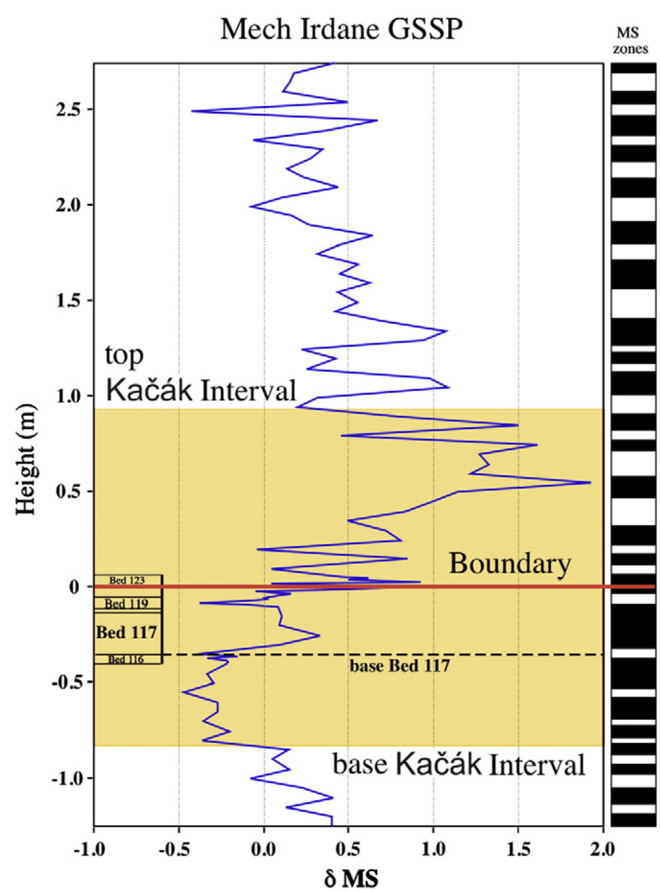

Fig. 4. δMS profile for the Mech Irdane GSSP expanded to cover the ~4 m of section containing the Kačák Interval. Included are the important bed numbers from Walliser et al. (1995). The MS zones (bar-log) to the right in the diagram represent the cyclicity in the section where open zones represent lower δMS values while filled zones represent higher δMS values. Observed MS zone cyclicity (~6 cycles/m) reflects the P2 precessional cyclic variations calculated for the section and presented in Fig. 3.

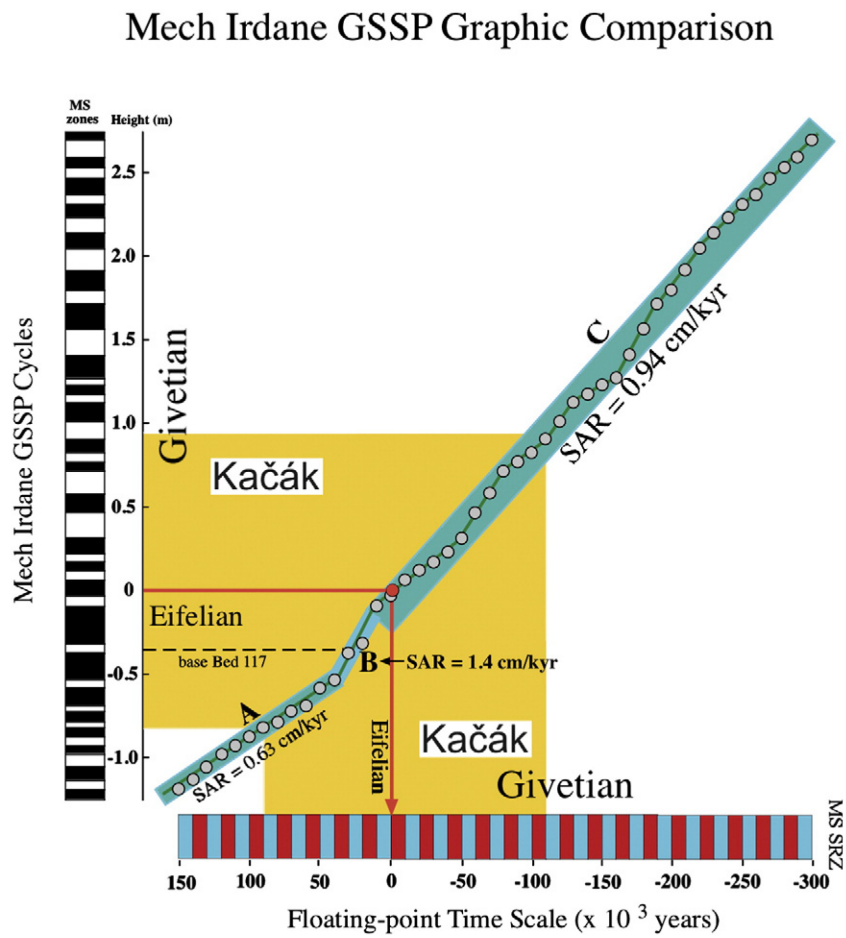

Fig. 5. Graphic comparison of a uniform floating-point time scale model MS standard reference zonation (MS SRZ) with the MS zones developed in Fig. 4. Also given are the boundary location, Kačák Interval and base of marl Bed 117. Data points represent the intersection of tops and bottoms of bar-log intervals from the raw δMS data and the model. The model is based on a P2 precession cyclicity of ~20 kyr, with each MS zone representing a P2 half cycle interval of ~10 kyr. Three trends (general lines of correlation, A, B, and C) were fit to the data and represent different (but internally uniform) sediment accumulation rates (SARs).

volume). The relative age and/or duration of these zones can then be correlated to other sections using MS zonation schemes developed for those sequences by comparison to the MS Standard Reference Zonation (MS SRZ) established here in Fig. 5. This then allows estimates of timing and consistency among globally distributed multiple biostratigraphic datasets.

Potentially, the FPTS developed above can be tied into an absolute time frame based on radiometric dating of the E–G boundary. Several studies have estimated the age of the E–G boundary, e.g., 381.8 Ma (Ogg et al., 2008), 387.5 Ma (Tucker et al., 1998), and 388.1 Ma (Kaufmann, 2006). The absolute time represented by any point in the FPTS can be calculated by assigning any of these dates to the E–G boundary in Fig. 5. For example, an age of 388.1 Ma for the E–G boundary (Kaufmann, 2006) yields an estimated start and end date for the Kačák Interval of 388.19 Ma and 387.99 Ma, respectively.

4.4. Chemostratigraphic data

Fig. 6 shows chemostratigraphic profiles for a ~10 m interval through the late Eifelian and early Givetian, and Fig. 7 provides an expanded view of the same profiles for a narrower ~1.2 m interval straddling the E–G boundary and located entirely within the Kačák Interval. Total organic carbon (TOC) concentrations are low throughout the study section (<0.12%; Fig. 6A), although there is a noticeable if slight enrichment below the E–G boundary in beds 116–119 (Fig. 7A). Total inorganic carbon (TIC) concentrations indicate that the study section consists mostly of slightly argillaceous limestones (TIC ~10%, versus 12% for pure $CaCO_3$; Fig. 6B), although the 20-cm interval represented by Bed 117 is distinctly marly (TIC 3–8%; Fig. 7B).

Carbonate $\delta^{13}C$ exhibits uniform values of +0.5 to +1.0‰ below the Kačák Interval and +1.5 to +2.0‰ above it (Fig. 6C). Thus, there is a systematic shift of about +1.0‰ associated with this event interval. This $\delta^{13}C$ shift is not associated with the E–G boundary itself but, rather, occurs earlier in the section, as the more positive values characteristic of the Givetian part of the section are found already in the uppermost ~15 cm of the Eifelian (Fig. 7C). The only interval in which carbonate $\delta^{13}C$ values do not fall within one of the narrow ranges noted above is within the 20-cm-thick marly layer of Bed 117. In this interval, $\delta^{13}C$ values are as low as −7.5‰, with the most ^{13}C-depleted values near the base of Bed 117 and a gradual trend toward less ^{13}C-depleted values upsection (Fig. 7C). This pattern is consistent with the independent C-isotopic results of Ellwood et al. (2003). Carbonate $\delta^{13}C$ exhibits a modest yet significant relationship to TOC, with more ^{13}C-depleted values associated with higher TOC concentrations ($r^2 = 0.28$; Fig. 8A).

Carbonate $\delta^{18}O$ values throughout the Mech Irdane section fall within a narrow range, mostly −10.8 to −11.4‰ (Fig. 6D), although values as high as −9.8‰ are encountered within Bed 117 (Fig. 7D). Although there is no significant relationship between $\delta^{18}O$ and $\delta^{13}C$ either below the base of Bed 117 or above the E–G boundary, the sample subset from the 38-cm-thick interval between these horizons exhibits highly significant negative covariation ($r^2 = 0.81$; Fig. 8A).

A variety of geochemical proxies exhibit slight to moderate increases and markedly stronger variance within and above the

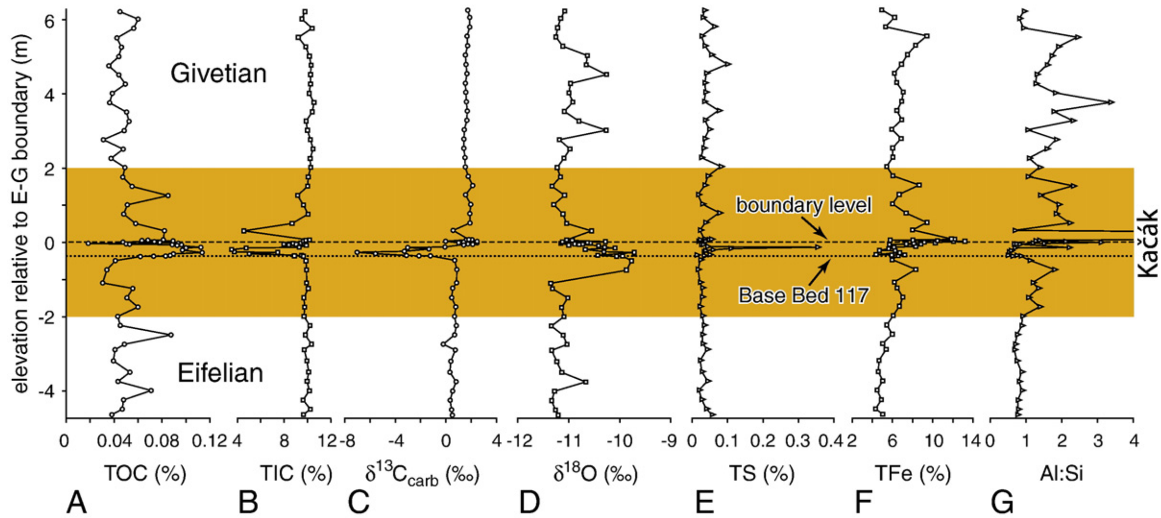

Fig. 6. Chemostratigraphic patterns in the Mech Irdane Eifelian–Givetian boundary GSSP section. (A) total organic carbon; (B) total inorganic carbon; (C) $\delta^{13}C_{carb}$; (D) $\delta^{18}O$; (E) total sulfur; (F) total iron (oxide weight); and (G) Al:Si (oxide weight ratio). The base of Bed 117 is ~38 cm below the Eifelian–Givetian boundary (Fig. 4). Shaded area represents the environmentally disturbed Kačák Interval (Fig. 2).

Kačák Interval, relative to the underlying beds. Total sulfur (TS) values are low throughout the section, except for a spike to >0.3% at the top of Bed 117 (Figs. 6E, 7E). Total iron (TFe) increases by an average of ~30% from the Kačák Interval upward, relative to the lower part of the section (Fig. 6F). Although Al and Si concentrations exhibit strong positive covariation throughout the section (e.g., Fig. 7F–G), Al:Si ratios change substantially upsection. Al:Si ratios increase by 50–100% and exhibit much stronger variance within and above the Kačák Interval, relative to the lower part of the section (Fig. 6G). The increase in Al:Si ratios is associated with the upper half of the Kačák Interval, from Bed 118 upward (Fig. 7H).

Trace-metal concentrations are generally low throughout the study section, although some beds within the Kačák Interval exhibit modest enrichments of Mo, U, and V; other metals, including Zn, Cu, Ni, Pb, and Cr, exhibit no systematic stratigraphic changes in concentration. Peaks in Mo and U concentrations are localized just below the base of Bed 117, where these metals increase by ~5× to 10× relative to background levels (Fig. 7I–J). A peak in V concentrations, ~5× higher than background levels, is found in the middle of Bed 117, about 15 cm above the peaks in Mo and U (Fig. 7K).

5. Discussion

5.1. The Kačák Interval

The Kačák Interval represents an important bio-event that has been discussed and redefined by a number of workers, resulting in some confusion regarding its defining characteristics and duration (Barnes et al., 1996; DeSantis et al., 2007; House, 1985, 2002; Schöne, 1997; Walliser, 1990, 1996, 1999; Walliser et al., 1995; see summary in Ellwood et al., 2011–this volume). However there is agreement that the onset of the Kačák Interval is associated with transgression and development of dysoxic or anoxic bottom waters at some time prior to the E–G boundary and that the more reducing conditions produced by this transgressive event were linked with coeval extinctions among marine taxa (Barnes et al., 1996; Walliser et al., 1995). This transgressive

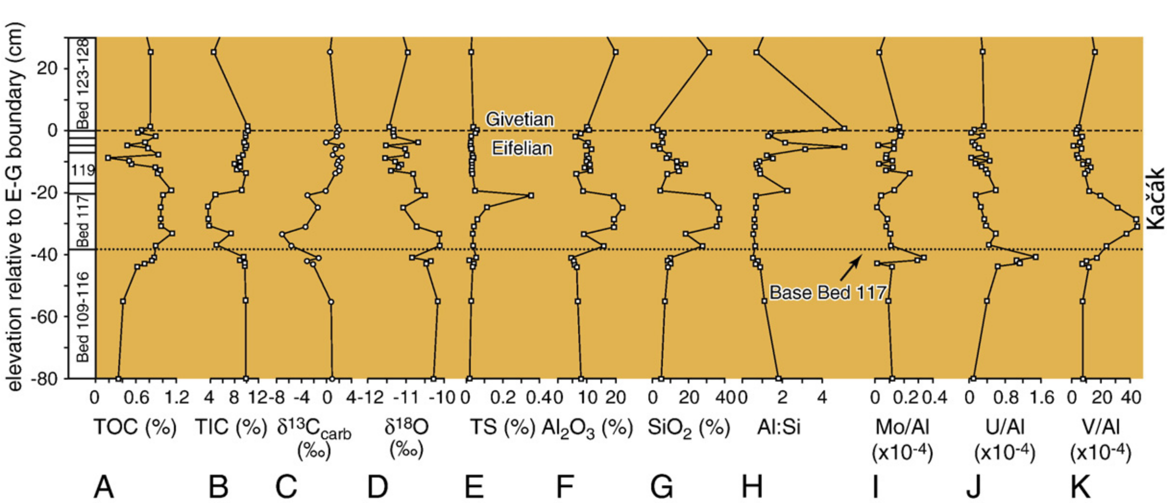

Fig. 7. Detail of chemostratigraphic patterns in the interval through the environmentally disturbed Kačák Interval within the Eifelian–Givetian boundary section (Fig. 2). (A) total organic carbon; (B) total inorganic carbon; (C) $\delta^{13}C_{carb}$; (D) $\delta^{18}O$; (E) total sulfur; (F) Al_2O_3; (G) SiO_2; (H) Al:Si (oxide weight ratio); (I) Mo/Al; (J) U/Al; and (K) V/Al. Also included are the bed number locations through the boundary interval (Walliser et al., 1995).

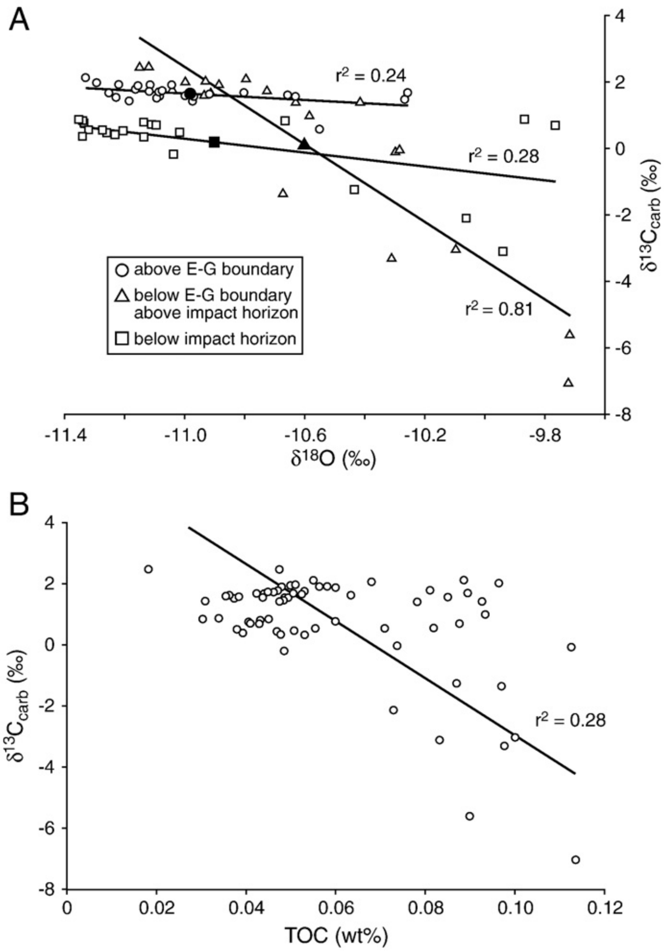

Fig. 8. (A) Carbonate $\delta^{13}C$–$\delta^{18}O$ crossplot. Symbols indicate the stratigraphic position of samples relative to the E–G boundary and Bed 117; solid symbols give the mean for each stratigraphic interval. Only the sample set between the base of Bed 117 and the E–G boundary exhibits significant covariation ($r^2=0.81$, $p(\alpha)<0.01$, d.f. = 20). (B) Carbonate $\delta^{13}C$ versus TOC. A subset of slightly TOC-enriched samples exhibits markedly ^{13}C-depleted isotopic compositions, yielding a significant correlation ($r^2=0.28$, $p(\alpha)<0.01$, d.f. = 67). All isotopic values are relative to the V-PDB standard.

event, which is marked by a major shift toward lower δMS below Bed 117 (Fig. 2), is thought to be equivalent to the onset of the stepped T/R cycle If of Johnson et al. (1985); see also Brett et al., 2011–this volume).

Although Walliser in several papers has restricted the Kačák to the latest Eifelian [*ensensis* Zone sensu stricto] (i.e., Walliser, 1990, 1996, 1999), House (2002) indicated that the Kačák Interval extended to slightly above the E–G GSSP boundary level. Our MS and geochemical data indicate that the Kačák Interval probably extends to almost a meter above the E–G boundary (Figs. 2–4), supporting House's (2002) interpretation. Further, the present study demonstrates the occurrence of geochemical anomalies below the base of Bed 117, as far as ~1 m below the E–G boundary, suggesting that the Kačák Interval commenced gradually and intensified as the E–G boundary was approached. Given the ramifications for contemporaneous marine environments and biotas, we propose that the Kačák Interval be extended to include the complete ~2 m-thick interval straddling the E–G boundary, as shown by shading in Figs. 2 and 4–7. In this context, it is possible that the Kačák Interval actually includes two or more environmental perturbations.

5.2. Diagenetic influences on sediment chemistry

Some aspects of the geochemistry of the Mech Irdane section record primarily diagenetic influences, which must be recognized in order to draw inferences concerning depositional conditions from the remaining data. The strongly ^{18}O-depleted composition of Mech Irdane carbonates (Fig. 6) indicates that they preserve no primary environmental information, and that minor variation in $\delta^{18}O$ was probably due to small, lithology-dependent differences in the timing and depth of formation of diagenetic phases (cf. Algeo et al., 1992). The ~7‰ negative C-isotopic excursion seen in Bed 117 (Fig. 7) is probably also of diagenetic origin, as shown by patterns of covariation with $\delta^{18}O$ and TOC (Fig. 8). A possible scenario is that Bed 117 originally contained larger amounts of organic carbon (hence its somewhat higher TOC values; Fig. 7A), and that oxidation of organic matter in the burial environment generated ^{13}C-depleted bicarbonate as well as increased alkalinity, resulting in earlier cementation of this layer and uptake of more isotopically light C into diagenetic phases, relative to underlying and overlying beds. If the oxidized organic matter had a $\delta^{13}C$ value of ca. −25‰ and the diagenetic system was more-or-less closed, then the pre-burial TOC content of the Bed 117 marly layer was ~1–3% (versus present concentrations of ~0.1%). Large negative excursions in $\delta^{13}C_{carb}$ are sometimes associated with the influence of meteoric waters (e.g., Algeo et al., 1992), although petrographic or field evidence for subaerial exposure at the level of Bed 117 is lacking. Other geochemical profiles may contain information concerning primary environmental conditions (see Section 5.3).

5.3. Eustatic and environmental changes associated with the Kačák Interval

The MS profile shows that short-term cyclicity that is superimposed on longer-term trends that we interpret as T/R sea level cycles (Fig. 2). Increasing δMS values from the base of the section (−4.5 m below the E–G boundary) to just below the Kačák Interval (−1.7 m) represent higher rates of detrital flux to the site, probably as a result of eustatic regression. Within the Kačák Interval, δMS values provide evidence of a T–R couplet, with a rapid transgressive phase from −1.7 m to −0.4 m followed by a rapid regressive phase from −0.4 m to 0.6 m. Decreasing δMS values over a ~7 m interval beginning near the top of the Kačák Interval (0.6 m) document an extended transgressive phase (Fig. 2). δMS values exhibit only limited variation from ~8 m to ~12 m, but decrease again near the top of the section, suggesting short-term transgressions in conjunction with the two *pumilio* beds. Throughout the section, short-term δMS cyclicity of probable climatic origin is superimposed on these longer-term T/R eustatic cycles.

The +1‰ shift in $\delta^{13}C_{carb}$ from the Eifelian to the Givetian at Mech Irdane may reflect an increase in the global burial flux of ^{13}C-depleted organic carbon, possibly due to sequestration of organic matter in black shales deposited elsewhere. A positive excursion in $\delta^{13}C_{carb}$ has been reported from many E–G boundary sections, although the magnitude of this excursion varies from <1‰, as in the Prague Syncline and the Carnic Alps (Buggisch and Mann, 2004) to ~+2‰ at Montagne Noire (Buggisch and Joachimski, 2006) and in the Eifel region (van Geldern et al., 2006). Such geographic variation implies some regional differences in watermass conditions related to, e.g., productivity or C_{org} burial rates, watermass exchange, or freshwater inputs. The excursion in $\delta^{13}C_{carb}$ values at the E–G boundary is thus similar in sign but smaller in magnitude to $\delta^{13}C$ changes reported from the Frasnian–Famennian (F–F) and Devonian–Carboniferous (D–C) boundaries (Buggisch and Joachimski, 2006; Buggisch et al., 2008; Joachimski et al., 2001, 2002), which have also been linked to major changes in the global carbon cycle.

Sulfur and trace-metal concentration data may provide information regarding redox conditions at Mech Irdane. Enrichments of these proxies exhibit a clear relationship to Bed 117: sulfur enrichment is limited to the top of this layer, V enrichment to its middle, and Mo and U enrichment mainly to beds just below this layer (Figs. 6 and 7). These patterns suggest control by redox conditions in the burial environment, with elemental enrichments mainly at redox boundaries within the sediment (cf. Morford et al., 2005; Thomson et al., 1995). A likely scenario is that H_2S was produced by sulfate-reducing bacteria consuming organic matter within Bed 117, and that this H_2S fluxed upward until it encountered iron concentrated at a redox boundary at the top of Bed 117, forming pyrite. Mo and U originally located in Bed 117 may have fluxed downward in the diagenetic environment until encountering a redox boundary at the base of this bed. V, being more immobile and strongly associated with clay minerals, remained concentrated within Bed 117 following initial accumulation (cf. Algeo and Maynard, 2004; Tribovillard et al., 2006). If Bed 117 originally contained 1–3% TOC (as inferred above), then it may have been deposited in a more reducing environment than the underlying and overlying beds, which accumulated under oxidizing conditions. In this regard, the E–G boundary may be similar to the F–F and D–C boundaries, which have also yielded geochemical and biomarker evidence of a short-term shift toward more reducing watermass conditions (Buggisch and Joachimski, 2006; Buggisch et al., 2008; Joachimski et al., 2001, 2002).

Concentration profiles for Fe, Al, and Si may provide information about primary chemical weathering fluxes to the Mech Irdane depositional system. Low, uniform concentrations of these elements below the base of Bed 117 suggest relatively stable conditions and uniform weathering fluxes prior to the Kačák Interval. Conversely, increases in the concentrations and variance of these elements from Bed 117 upward suggest higher and more variable weathering fluxes. Al:Si ratios provide an indication of changes in detrital grain size, with higher ratios associated with an increase in Al-bearing clays relative to Si-rich quartz silt. Although the concentrations of all detrital elements increase in Bed 117, the rise in Si (~7×) exceeds that in Al (~2×), resulting in the lowest Al:Si ratios in the Mech Irdane section (Fig. 6). This pattern may reflect greater influx of a coarser siliciclastic fraction in response to a coeval eustatic regression and is consistent with the higher δMS values observed in Bed 117 (Figs. 2 and 4). Al:Si ratios rise sharply in the 20-cm interval between Bed 117 and the E–G boundary and remain high but variable through the remainder of the section. This may reflect a sustained increase in chemical weathering intensity above the Kačák Interval, as reflected in higher average sedimentation rates for the Givetian (0.94 cm kyr^{-1}) relative to the Eifelian (0.63 cm kyr^{-1}; Fig. 5). Finer grain size (and, hence, higher Al:Si ratios) might also result from eustatic transgression as a consequence of sequestration of coarser detrital material in proximity to a receding shoreline, but this mechanism would generally result in lower sedimentation rates, not higher, as observed at Mech Irdane. Although Diener et al. (1996) inferred an interval of non-deposition or condensation at the E–G boundary, our data suggest that sedimentation rates transiently increased (by a factor of ~2×) during deposition of Bed 117, the middle of the Kačák Interval (Fig. 5).

Evidence for a eustatic regression and enhanced weathering fluxes at the E–G boundary implies concurrent global climatic cooling and an increase in continental ice volume. Existing brachiopod and conodont O-isotope data do not provide any evidence for a significant temperature change across the E–G boundary, in contrast to the pronounced short-term cooling events that characterize the Givetian–Frasnian (G–F), F–F, and D–C boundaries (Buggisch et al., 2008; Joachimski and Buggisch, 2002; Joachimski et al., 2004; van Geldern et al., 2006). However, the similarities among the geochemical records of these boundary events noted above, e.g., enhanced organic carbon burial in conjunction with more reducing conditions, suggest that they had similar causes and consequences. Short-term cooling at the E–G boundary may have been masked by the generally cool conditions that prevailed in the Middle Devonian, during which tropical marine temperatures were ~5 to 10 °C lower than during the Early or Late Devonian (Joachimski et al., 2009). In summary, the E–G boundary probably reflects a large-scale marine anoxic/organic carbon burial event of the same type that characterizes the G–F, F–F, and D–C boundaries. The ultimate cause(s) of these events remain unknown but may be connected to the spread of vascular land plants (Algeo and Scheckler, 1998; Algeo et al., 1995) and/or to episodes of greater tectonic activity (Averbuch et al., 2004; Riquier et al., 2005).

5.4. Significance of the pumilio beds

In the upper part of the almost exclusively carbonate sequence at Mech Irdane are the distinctive "*Terebratula*" *pumilio* beds, two marly layers each ~0.2 m-thick, that are separated by ~2 m of limestone (Fig. 2). These beds contain high concentrations of small, "*T.*" *pumilio* brachiopods that were postulated to have been brought to the site by tsunami events (Lottmann, 1990a,b). Alternatively, Brett and Baird (1997) suggested that these beds reflect shell concentrations during sediment starvation at flooding surfaces. Decreasing δMS values within the Mech Irdane GSSP from the E–G boundary upward indicate long-term transgression, and each *pumilio* layer is associated with some of the lowest δMS values in the section. We interpret these low values to represent sediment starvation surfaces developed at maximum flooding surfaces. We hypothesize that a long-term deepening event (transgression) above the E–G boundary may have provided environmental conditions that allowed high *pumilio* productivity while simultaneously reducing detrital fluxes to the marine environment. These conditions yielded fossil-rich beds with very low δMS values as a consequence of sediment starvation, as suggested by Brett and Baird (1997).

6. Conclusions

We report new results from magnetic susceptibility (MS) and geochemical analyses of the Middle Devonian Eifelian–Givetian GSSP located at Mech Irdane, in the Anti-Atlas Mountains of Morocco. Fourier analysis of the MS profile from the study section yielded high power at four frequencies that are consistent with Milankovitch–band orbital forcing: eccentricity (E1 and E2) at ~400 and ~100 kyr, obliquity (O1) at ~32 kyr, and precession (P2) at ~20 kyr, the latter two corrected for secular changes in Earth's orbit since the Middle Devonian. Based on these results, a high-resolution floating-point time scale was developed for the late Eifelian–early Givetian Interval. This time scale allows a temporal resolution of ~10 kyr within the study section and demonstrates that the Kačák event, which spans a ~2.0 m stratigraphic interval at Mech Irdane, had a duration of ~200 ± 10 kyr.

Based on observed MS and geochemical patterns, the Mech Irdane section records a broad eustatic regression from its base to just below the Kačák Interval. The Kačák Interval itself contains a rapid transgressive–regressive couplet and is characterized by more reducing conditions, greater organic carbon burial, and an increase in the flux of detrital materials (especially clays), all of which may have been a consequence of enhanced subaerial weathering. A major eustatic transgression commences near the top of the Kačák Interval and continues through the upper 14 m of the section. Two regional (or perhaps global) bio-event beds in the lower Givetian, the Lower and Upper "*Terebratula*" *pumilio* beds, coincide with maximum flooding surfaces near the top of the section. These epibole horizons may represent a unique environment allowing high productivity and rapid proliferation of the small *pumilio* brachiopods at times of reduced detrital sediment flux.

Acknowledgements

This work was funded in part by grants to R.E. Crick and B. Ellwood from the National Science Foundation (NSF; EAR-9628202) and the American Chemical Society PRF (#30845-AC8 and #34259-AC8) and by grants to TJA from the National Science Foundation (EAR-0618003 and EAR-0745574). We wish to thank Suzanne Ellwood for her important contribution to this work in designing the sampling method used in collecting our samples, for her participation in collecting all of the Moroccan samples reported here, and for other significant contributions to the work. This paper is a contribution to IGCP Project 499. We are grateful to Eberhard Schindler and Anne-Christine da Silva for their constructive reviews of the manuscript.

References

Algeo, T.J., Maynard, J.B., 2004. Trace element behavior and redox facies in core shales of Upper Pennsylvanian Kansas-type cyclothems. Chemical Geology 206, 289–318.

Algeo, T.J., Scheckler, S.E., 1998. Terrestrial-marine teleconnections in the Devonian: links between the evolution of land plants, weathering processes, and marine anoxic events. Royal Society of London Philosophical Transactions B353, 113–130.

Algeo, T.J., Wilkinson, B.H., Lohmann, K.C., 1992. Meteoric-burial diagenesis of Pennsylvanian carbonate: water/rock interactions and basin geothermics. Journal of Sedimentary Petrology 62, 652–670.

Algeo, T.J., Berner, R.A., Maynard, J.B., Scheckler, S.E., 1995. Late Devonian oceanic anoxic events and biotic crises: "rooted" in the evolution of vascular land plants? GSA Today 5 (45), 64–66.

Algeo, T.J., Hannigan, R., Rowe, H., Brookfield, M., Baud, A., Krystyn, L., Ellwood, B.B., 2007. Sequencing events across the Permian–Triassic boundary, Guryul Ravine (Kashmir, India). Palaeogeography Palaeoclimatology Palaeoecology 252, 328–346.

Averbuch, O., Tribovillard, N., Devleeschouwer, X., Riquier, L., Mistiaen, B., van Vliet-Lanoe, B., 2004. Mountain building-enhanced continental weathering and organic carbon burial as major causes for climatic cooling at the Frasnian–Famennian boundary (c. 376 Ma)? Terra Nova 17, 25–34.

Barnes, C., Hallam, A., Kaljo, D., Kauffman, E.G., Walliser, O.H., 1996. Global event stratigraphy. In: Walliser, O.H. (Ed.), Global Events and Event Stratigraphy. Springer Verlag, Berlin, pp. 225–250.

Berger, A., Loutre, M.F., Laskar, J., 1992. Stability of the astronomical frequencies over the Earth's history for paleoclimate studies. Science 255, 560–566.

Boulila, S., Hinnov, L.A., Huret, E., Colling, P.-Y., Galbrun, B., Fortwengler, D., Marchand, D., Thierry, J., 2008. Astronomical calibration of the Early Oxfordian (Vocontian and Paris basins, France): consequences of revising the Late Jurassic time scale. Earth and Planetary Science Letters 276, 40–51.

Brett, C.E., Baird, G.C., 1997. Epiboles, outages, and ecological evolutionary bioevents: taphonomic, ecological, and evolutionary factors. In: Brett, C.E., Baird, G.C. (Eds.), Paleontological Events: Stratigraphic, Ecological, and Evolutionary Implications. Columbia University Press, New York, pp. 249–285.

Brett, C.E., Baird, G., Bartholomew, A.J., DeSantis, M.K., Ver Straeten, C.A., 2011. Sequence stratigraphy and a revised sea-level curve for the Middle Devonian of eastern North America. Palaeogeography, Palaeoclimatology, Palaeoecology 304, 21–53 (this volume).

Buggisch, W., Joachimski, M.M., 2006. Carbon isotope stratigraphy of the Devonian of Central and Southern Europe. Palaeogeography, Palaeoclimatology, Palaeoecology 240, 68–88.

Buggisch, W., Mann, U., 2004. Carbon isotope stratigraphy of Lochkovian to Eifelian limestones from the Devonian of central and southern Europe. International Journal of Earth Sciences 93, 521–541.

Buggisch, W., Joachimski, M.M., Sevastopulo, G., Morrow, J.R., 2008. Mississippian $\delta^{13}C_{carb}$ and conodont apatite $\delta^{18}O$ records—their relation to the Late Palaeozoic Glaciation. Palaeogeography, Palaeoclimatology, Palaeoecology 268, 273–292.

Crick, R.E., Ellwood, B.B., El Hassani, A., Feist, R., 2000. Proposed magnetostratigraphy susceptibility magnetostratotype for the Eifelian–Givetian GSSP (Anti-Atlas Morocco). Episodes 23, 93–101.

Crick, R.E., Ellwood, B.B., El Hassani, A., Hladil, J., Hrouda, F., Chlupáč, I., 2001. Magnetostratigraphy susceptibility of the Pridoli–Lochkovian (Silurian–Devonian) GSSP (Klonk, Czech Republic) and a coeval sequence in Anti-Atlas Morocco. Palaeogeography, Palaeoclimatology, Palaeoecology 167, 73–100.

da Silva, A.-C., Boulvain, F., 2002. Sedimentology, magnetic susceptibility and isotopes of a Middle Frasnian carbonate platform: Tailfer Section, Belgium. Facies 46, 89–102.

DeSantis, M.K., Brett, C.E., Ver Straeten, C.A., 2007. Persistent depositional sequences and bioevents in the Eifelian (early Middle Devonian) of eastern Laurentia: North America. Evidence of the Kačák Events? In: Becker, R.T., Kirchgasser, W.T. (Eds.), Devonian Events and Correlations. Special Publications, 278. Geological Society of London, pp. 83–104.

Dettinger, M.D., Ghil, M., Strong, C.M., Weibel, W., Yiou, P., 1995. Software expedites singular-spectrum analysis of noisy time series. Eos, Transactions of the American Geophysical Union 76, 12–21.

Diener, A., Ebneth, S., Veizer, J., Buhl, D., 1996. Strontium isotope stratigraphy of the Middle Devonian: brachiopods and conodonts. Geochimica et Cosmochimica Acta 60, 639–652.

Dinarès-Turell, J., Baceta, J.I., Bernaola, G., Orue-Etxebarria, X., Pujalte, V., 2007. Closing the Mid-Palaeocene gap: toward a complete astronomically tuned Palaeocene Epoch and Selandian and Thanetian GSSPs at Zumaia (Basque Basin, W Pyrenees). Earth Planetary Science Letters 262, 450–467.

Ellwood, B.B., Crick, R.E., El Hassani, A., Benoist, S.L., Young, R.H., 2000. The magnetosusceptibility event and cyclostratigraphy (MSEC) method applied to marine rocks: detrital input versus carbonate productivity. Geology 28, 1134–1138.

Ellwood, B.B., Benoist, S.L., El Hassani, A., Wheeler, C., Crick, R.E., 2003. Impact ejecta layer from the Mid-Devonian: possible connection to global mass extinctions. Science 300, 1734–1737.

Ellwood, B.B., Brett, C.E., MacDonald, W.D., 2007a. Magnetosusceptibility stratigraphy of the Upper Ordovician Kope Formation, Northern Kentucky. Palaeogeography, Palaeoclimatology, Palaeoecology 243, 42–54.

Ellwood, B.B., Tomkin, J., Richards, B., Benoist, S.L., Lambert, L.L., 2007b. MSEC data sets record glacially driven cyclicity: examples from the Arrow Canyon Mississippian–Pennsylvanian GSSP and associated sections. Palaeogeography, Palaeoclimatology, Palaeoecology 255, 377–390. doi:10.1016/j.palaeo.2007.08.006.

Ellwood, B.B., Tomkin, J.H., Febo, L.A., Stuart Jr., C.N., 2008a. Time series analysis of magnetic susceptibility variations in deep marine sediments: a test using Upper Danian–Lower Selandian proposed GSSP, Spain. Palaeogeography, Palaeoclimatology, Palaeoecology 261, 270–279.

Ellwood, B.B., Tomkin, J.H., Ratcliffe, K.T., Wright, M., Kafafy, A.M., 2008b. High resolution magnetic susceptibility and geochemistry for the Cenomanian/Turonian boundary GSSP with correlation to time equivalent core. Palaeogeography, Palaeoclimatology, Palaeoecology 261, 105–126.

Ellwood, B.B., Tomkin, J.H., El Hassani, A., Bultynck, P., Brett, C.E., Schindler, E., Feist, R., Bartholomew, A., 2011. A climate-driven model and development of a floating point time scale for the entire Middle Devonian Givetian Stage: a test using magnetostratigraphic susceptibility as a climate proxy. Palaeogeography, Palaeoclimatology, Palaeoecology 304, 85–95 (this volume).

Gale, A.S., Voigt, S., Sageman, B.B., Kennedy, W.J., 2008. Eustatic sea-level record for the Cenomanian (Late Cretaceous)-extension to the Western Interior Basin, USA. Geology 36, 859–862.

Ghil, M., Allen, R.M., Dettinger, M.D., Ide, K., Kondrashov, D., Mann, M.E., Robertson, A., Saunders, A., Tian, Y., Varadi, F., Yiou, P., 2002. Advanced spectral methods for climatic time series. Reviews in Geophysics 40 (1), 3.1–3.41. doi:10.1029/2000RG000092.

Hartl, P., Tauxe, L., Herbert, T., 1995. Earliest Oligocene increase in South Atlantic productivity as interpreted from "rock magnetics" at Deep Sea drilling Site 522. Paleoceanography 10, 311–326.

House, M.R., 1985. Correlation of mid-Palaeozoic ammonoids evolutionary events with global sedimentary perturbations. Nature 313, 17–22.

House, M.R., 2002. Strength, timing, setting and cause of mid-Palaeozoic extinctions. Palaeogeography, Palaeoclimatology, Palaeoecology 181, 5–25.

Imbrie, J., Hays, J.D., Martinson, D.G., McIntyre, A., Mix, A.C., Morley, J.J., Pisias, N.G., Prell, W.L., Shackleton, N.J., 1984. The orbital theory of Pleistocene climate: support from a revised chronology of the marine delta ^{18}O record. In: Berger, A.L., Imbrie, J., Hays, J., Kukla, G., Saltzman, B. (Eds.), Milankovitch and Climate, Part I. Kluwer Academic Publishers, Dordrecht, pp. 269–305.

Jenkins, G.M., Watts, D.G., 1968. Spectral Analysis and its Applications. Holden-Day, San Francisco. 525 pp.

Joachimski, M.M., Buggisch, W., 2002. Conodont apatite $\delta^{18}O$ signatures indicate climatic cooling as a trigger of the Late Devonian mass extinction. Geology 30, 711–714.

Joachimski, M.M., Ostertag-Henning, C., Pancost, R.D., Strauss, H., Freeman, K.H., Littke, R., Sinninghe Damsté, J.S., Racki, G., 2001. Water column anoxia, enhanced productivity and concomitant changes in $\delta^{13}C$ and $\delta^{34}S$ across the Frasnian–Famennian boundary (Kowala—Holy Cross Mountains/Poland). Chemical Geology 175, 109–131.

Joachimski, M.M., Pancost, R.D., Freeman, K.H., Ostertag-Henning, C., Buggisch, W., 2002. Carbon isotope geochemistry of the Frasnian–Famennian transition. Palaeogeography, Palaeoclimatology, Palaeoecology 181, 91–109.

Joachimski, M.M., van Geldern, R., Breisig, S., Buggisch, W., Day, J., 2004. Oxygen isotope evolution of biogenic calcite and apatite during the Middle and Late Devonian. International Journal of Earth Sciences 93, 542–553.

Joachimski, M.M., Breisig, S., Buggisch, W., Talent, J.A., Mawson, R., Gereke, M., Morrow, J.R., Day, J., Weddige, K., 2009. Devonian climate and reef evolution: insights form oxygen isotopes in apatite. Earth and Planetary Science Letters 284, 599–609.

Johnson, J.G., Klapper, G., Sandberg, C.A., 1985. Devonian eustatic fluctuations in Euramerica. Geological Society of America Bulletin 96, 567–587.

Kaufmann, B., 2006. Calibrating the Devonian time scale: a synthesis of U–Pb ID-TIMS ages and conodont stratigraphy. Earth-Science Reviews 76, 175–190.

Laskar, J., Robutel, P., Joutel, F., Gastineau, M., Correia, A., Levrard, B., 2004. A long-term numerical solution for the insolation quantities of the Earth. Astronomy and Astrophysics 428, 261–285.

Lottmann, J., 1990a. Die pumilio-Events (Mittel-Devon). Gottinger Arbeiten zur Geologie und Paläontologie 44, 99 pp.

Lottmann, J., 1990b. The Middle Givetian *pumilio*-Events a tool for high resolution and event-stratigraphical correlation. In: Kauffmann, E.G., Walliser, O.H. (Eds.), Extinction Events in Earth History, 30, pp. 145–149.

Mead, G.A., Tauxe, L., LaBrecque, J.L., 1986. Oligocene paleoceanography of the South Atlantic: paleoclimate implications of sediment accumulation rates and magnetic susceptibility. Paleoceanography 1, 273–284.

Morford, J.L., Emerson, S.R., Breckel, E.J., Kim, S.H., 2005. Diagenesis of oxyanions (V, U, Re, and Mo) in pore waters and sediments from a continental margin. Geochimica et Cosmochimica Acta 69, 5021–5032.

Ogg, J.G., Ogg, G., Gradstein, F.M., 2008. The Concise Geologic Time Scale. Cambridge University Press, England. 177 pp.

Olsen, P.E., Kent, D.V., 1995. Milankovitch climate forcing in the tropics of Pangaea during the Late Triassic. Palaeogeography, Palaeoclimatology, Palaeoecology 122, 1–26.

Riquier, L., Tribovillard, N., Averbuch, O., Joachimski, M.M., Racki, G., Devleeschouwer, X., El Albani, A., Riboulleau, A., 2005. Productivity and bottom water redox conditions at the Frasnian–Famennian boundary on both sides of the Eovariscan Belt: constraints from trace-element geochemistry. In: Over, D.J., Morrow, J.R., Wignall, P.B. (Eds.), Understanding Late Devonian and Permian–Triassic Biotic and Climatic Events. Elsevier, Amsterdam, pp. 199–224.

Schmitz, B., Ellwood, B.B., Peucker-Ehrenbrink, B., El Hassani, A., Bultynck, P., 2006. Platinum group elements and $^{187}Os/^{188}Os$ in a purported impact ejecta layer near Eifelian–Givetian stage boundary, Middle Devonian. Earth and Planetary Science Letters 249, 162–172.

Schöne, B.R., 1997. Der *otomari*-Event und seine Auswirkungen auf die Fazies des Rhenoherzynischen Schelfs (Devon, Rheinisches Schiefergebirge). Göttinger Arbeiten zur Geologie und Paläontologie 70, 140 pp.

Shackleton, N.J., McCave, I.N., Weedon, G.P., 1999a. Preface. Philosophical Transactions of the Royal Society London, A 357, 1733–1734.

Shackleton, N.J., Crowhurst, S.J., Weedon, G.P., Laskar, J., 1999b. Astronomical calibration of Oligocene–Miocene time. Philosophical Transactions of the Royal Society London, A 357, 1907–1929.

Shaw, A.B., 1964. Time in Stratigraphy. New York, McGraw Hill. 365 pp.

Swartzendruber, L.J., 1992. Properties, units and constants in magnetism. Journal of Magnetic Materials 100, 573–575.

Thomson, J., Higgs, N.C., Wilson, T.R.S., Croudace, L.W., de Lange, G.J., van Santvoort, P.J.M., 1995. Redistribution and geochemical behavior of redox-sensitive elements around S1, the most recent eastern Mediterranean sapropel. Geochimica et Cosmochimica Acta 59, 3487–3501.

Tribovillard, N., Algeo, T.J., Lyons, T.W., Riboulleau, A., 2006. Application of trace metals as paleoredox and paleoproductivity proxies. Chemical Geology 232, 12–32.

Tucker, R.D., Bradley, D.C., Ver Straeten, C.A., Harris, A.G., Ebert, J.R., McCutcheon, S.R., 1998. New U–Pb zircon ages and the duration and division of Devonian time. Earth and Planetary Science Letters 158, 175–186.

van Geldern, R., Joachimski, M.M., Day, J., Jansen, U., Alvarez, F., Yolkin, E.A., Ma, X.-P., 2006. Carbon, oxygen and strontium isotope records of Devonian brachiopod shell calcite. Palaeogeography, Palaeoclimatology, Palaeoecology 240, 47–67.

Walliser, O.H., 1990. How to define "Global Bio-Events". In: Kauffman, E.G., Walliser, O.H. (Eds.), Extinction Events in Earth History. Lecture Notes in Earth Sciences, 30. Springer Verlag, Berlin, pp. 1–3.

Walliser, O.H., 1991. Jebel Mech Irdane (Mapsheet Erfoud, NH-30-XX-2). In: Walliser, O.H. (Ed.), Morocco, Field Meeting of the Subcommission on Devonian Stratigraphy, pp. 25–47.

Walliser, O.H., 1996. Global events in the Devonian and Carboniferous. In: Walliser, O.H. (Ed.), Global Events and Event Stratigraphy. Springer Verlag, Berlin, pp. 225–250.

Walliser, O.H., 1999. The Jebel Mech Irdane section: SDS-IGCP 421 Morocco Meeting. Field Trip Excursion Guidebook, pp. 65–71.

Walliser, O.H., Bultynck, P., Weddige, K., Becker, R.T., House, M.R., 1995. Definition of the Eifelian–Givetian Stage boundary. Episodes 18, 107–115.

Weedon, G.P., Shackleton, N.J., Pearson, P.N., 1997. The Oligocene time scale and cyclostratigraphy on the Ceara Rise, western equatorial Atlantic. In: Schackleton, N.J., Curry, W.B., Richter, C., Bralower, T.J. (Eds.), Proceedings of the Ocean Drilling Program, Scientific Results, vol. 154, pp. 101–114. 5.

Weedon, G.P., Jenkyns, H.C., Coe, A.L., Hesselbo, S.P., 1999. Astronomical calibration of the Jurassic time-scale from cyclostratigraphy in British mudrock formations. Philosophical Transactions of the Royal Society London, A 357, 1787–1813.

Whalen, M.T., Day, J.E., 2008. Magnetic susceptibility, biostratigraphy, and sequence stratigraphy: insights into Devonian carbonate platform development and basin infilling, Western Alberta. In: Lukasik, J., Simo, J.A. (Eds.), Papers on Phanerozoic Reef Carbonates in Honor of Wolfgang Schlager. Special Publication, 89. SEPM (Society for Sedimentary Geology, pp. 291–314.